Int. J. Electrochem. Sci., 17 **(2022)** Article Number: 221123, doi: 10.20964/2022.11.19

International Journal of
ELECTROCHEMICAL
SCIENCE
www.electrochemsci.org

Flow and Species Distribution Characteristics in a 15-cells Proton Ceramic Fuel Cell Stack with the Inter-Parallel Flow Field Channel by 3D Modeling

Z.F. Yuan[1,2], Y.D. Akenteng[2,], A.P. Shigwedha[2], X.L. Yang[2], D.F. Chen[2]*

[1] College of Aerospace Engineering, Nanjing University of Aeronautics and Astronautics, Nanjing 210016, China
[2] School of Energy and Power, Jiangsu University of Science and Technology, Zhenjiang 212100, China
[*]E-mail: fastestdwamena@yahoo.com

Received: 1 August 2022 / *Accepted:* 1 September 2022 / *Published:* 10 October 2022

The protonic ceramic fuel cell (PCFC) has attracted great attentison due to its many advantages at the intermediate working range. In this paper, the 3D calculated fluid dynamic (CFD) model for a planar 15-cells PCFC stack with a new inter-parallel flow field has been developed to evaluated its performance. Then, the dependence of the flow and speices distributing characteristics withint the PCFC stack on the structure parameters, such as the flowing arrangemen configurations, under-rib convection and no under-rib convection, the rib channel geometry, and so on, are studied. The calculated result shows that the three types subpathes within the new inter-parallel flow field design will enhance the under-rib convecting process and greatly improve the stack performance. Combined with the U-type air flow path and proper rib channel depth, the inter-parallel flow field not only can ensure high uniformities of the the flow and speices distribuitons for the PCFC stack, but also can greatly improving the water removing capacity capacity at a low-pressure drop.

Keywords: Proton Ceramic Fuel Cells, Computational Fluid Dynamics (CFD), Inter-Parallel Flow Field, Stack structure.

1. INTRODUCTION

In the drive to deliver clean energy as a solution to thep problem of depletion and over-reliance of fossil fuels and the impacts of emissions, proton ceramic fuel cells (PCFCs) have emerged as a viable intermediate temperature power generation alternative [1, 2]. Moreover, in PCFCs, water vapor is created at the cathode side instead of the anode side, which is quite different from the traditional solid oxide fuel cell basing on oxygen ion (O-SOFC) [3-5]. The PCFC offers numerous special benefits over

the other type fuel cells in the medium temperature range [6-8]. Great efforts have been addressed to numerical research areas of the fuel cell technologies. The design of a stack has been at the forefront [9]. The electromotive forces of the thermodynamic reaction of most hydrogen fuel cells are only around 1.0 V. Practically, this output voltage decreases due to the resistances of the electric charge and species transporting within the fuel cell stack. In addition, different fuels may result in varied reversible voltages because of their different properties. Thus, a fuel cell has a operation voltage around 0.5-0.8 volt [10-12].

It is necessary to note that a fuel cell stack performance is not simply determined by the sum of its individual cells, because of a variety of circumstances, such as the uneven distribution of reactants in the multiple stacks. The consequences of poor or maldistribution reactants are considered a critical issue in the fuel cell stack. Lack of uniformity in the membrane's current density results in localized hot patches, deterioration in performance, and degradation of the material [13]. On the other hand, uniform distribution results in better oxygen transport, water removal, and less mechanical stress on the membrane electrode assembly. D. Chen developed a broad regulation for the planar O-SOFC airflow distribution characteristics [14]. Choosing proper a flow field pattern is critical due to its impact on fuel cell performance in the stack environment. Many researchers have delved into improving the design of the flow field to improve fuel cell performance through theory, numerical or experimental methods. The 3D large-scale multiphysics modelling has been considered to be a proper approach for effectively studing the stack's flow, species, heat, electron, and ion transports [15].

Ref. [14] used actual solid, space, and porous architectures of a specifically 24-cells SOFC stack to investigate the multiphysics items distribution characteristics and affecting key structural parameters within the stack by 3D calculated fluid dynamics (CFD) modeling. In additiona, studies had investigated the impacts of various topologies, geometric characteristics, and species distribution properties inside cathode components on the stack performance [15]. However, it does not appear easy to establish a good flow field pattern to optimize water management, uniform electric current distribution, and high power density [16, 17]. Firstly, flow field flooding should be addressed by effectively removing accumulated water and produce high performance [18]. Generally, in contrast to the parallel flow field, the serpentine flow field had a longer channel length and many turns, which resulted in a greater pressure drop than that in the parallel flow field [19]. This design flaw maked the serpentine flow field a less desirable option. Even with high flow distribution benefits, there was still a risk of flooding in the areas around the outlet and the U-bend [19]. The interdigitated design was investigated by a 3D CFD model to investigate its distribution quality within a one-cell stack [20]. The design collaborated well with the multiphysics but did not address the pressure and water removal balance. Therefore, scientists have been finding the ideal balance between pressure drop and water removal. Under-rib convection was proved to be crucial for managing water [21-24]. It determined how successfully the catalyst layer was employed and the water removing capacity of the stacks [25-27]. In addition, as there was a direct relationship between the geometry and the under-rib convection, the implications of geometric design on the water management was also be studied [28].

In this paper, the cathodic flow characteristics of a 3D CFD modeled stack with the inter-parallel flow field. Firstly are studied. Then the stack with U and Z type configurations and the inter-parallel

stacks with under-rib flow field and no under-rib flow field are compard and discussed. Finally, the channel depth is varied to obtain optimal sizing for the model.

2. STRUCTURE AND THE THEORY

Fig. 1a shows the structure of the inter-parallel flow flied over the porous electrode of PCFC stack [29]. It consists of three types of subpathes running from the inlet to the outlet. As illustrated in **Fig. 1b,** the interdigitated dead zone characteristic is also incorporated into the design. Consequently, there is a disconnect between the inlet and the outlet on two subpaths. According to the inter-parallel design, subpath three is responsible for transporting oxygen, while path two is responsible for removing water. The subpath one contributes to the transportation of oxygen and the elimination of water. This design will takes advantage of the attributes of these flow fields. A PCFC stack stack using this flow filed structure, water would be effectively removed, and oxygen is diffused at a relatively low-pressure loss. Thus, the inter-parallel flow field with the under-rib convection will be modeled into a stack configuration. The design variations with the under-rib convection are shown in **Fig 1c.**

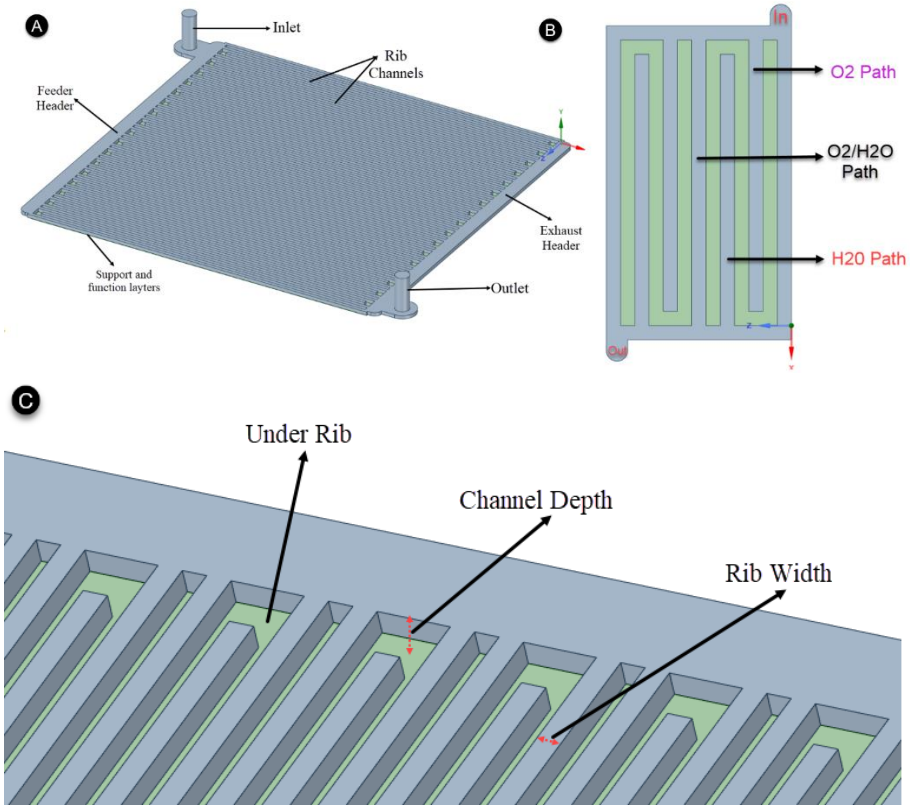

Figure 1. Inter-parallel flow field design: a) 3D image of the inter-parallel flow field; b) 2D image of the inter-parallel flow field; c) Variations in airflow channel design at the cathode: a picture illustrating channel width, channel depth, and rib width.

Fig. 2 delineates the 3D diagram of a PCFC stack design with the inter-parallel flow field. Characteristically, anode support, anode function, dense electrolyte, cathode function, and cathode current collector layers make up a PCFC stack. This work design model includes a 15 cells stack with 1 inlet and 1 outlet manifolds (labeled as 1in-1out) and the manifold radius of 4 mm. The corresponding reactions zone of each PCFC unti is 100 x 100 mm^2.

The U and Z type configurations are the most common airflow channel structures for fuel cell stacks. The inlet and outlet manifolds are located on the same side for the U, as shown in **Fig. 3a**; and on the opposing sides for the Z, as shown in **Fig. 3b**. The inter-parallel design in this work support both the U and the Z type configurations.

The 3D view of **Fig. 1c** shows the design alteration in flow channel width and depth. The channel depth was adjusted to offer a restricted passage to ensure a uniform flow distribution in the inter-parallel design. The inter-parallel design ensures uniform flow while maintaining a low pressure drop. The geometric and operational parameters for the current design are listed in **table 1.**

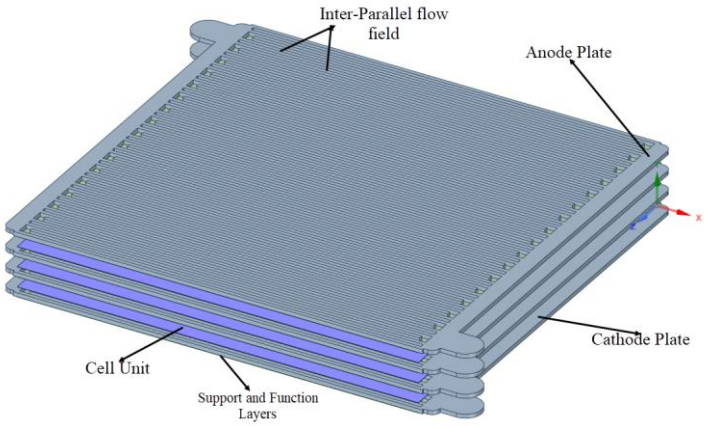

Figure 2. A typical PCFC stack with inter-parall flow field.

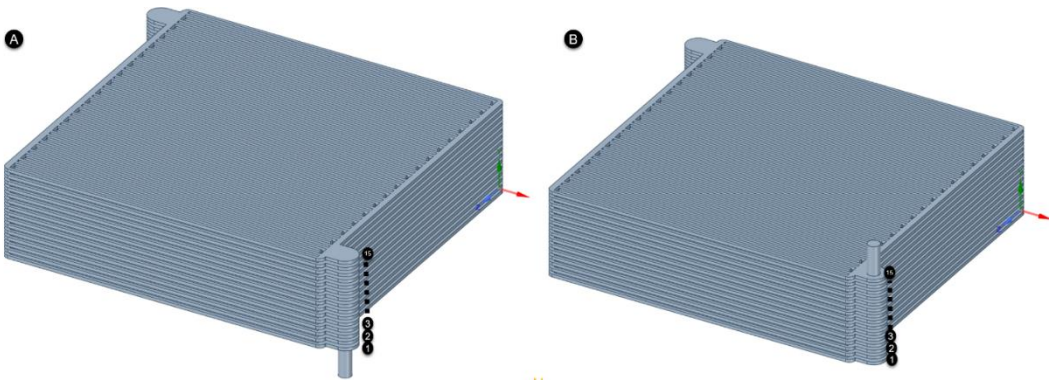

Figure 3. 3D CFD models for the cathode side of the 15-cells PCFC stack: a) U-type configuration, b) Z-type configuration.

Table 1. The geometric and operational parameters referring to the stack structure in **Figure 2**.

MEA area	100×100 mm²
Channel Width	1.0 mm
Channel Depth	0.9, 0.7,0.5,0.1 mm
Rib Width	1.0 mm
The cathode support layer thickness	0.05 mm
The cathode function layer thickness *l*	0.01 mm
Radius of air inlet manifolds	4.0 mm
Radius of air outlet manifolds	4.0 mm
Layer height	10.0 mm
The working temperature of PCFC	873.15 K
Output current density i_{op}	5000 A·m^{-2}
The oxygen utilization	0.2

The 3D model is simplified to the cathode side of the 15-cells PCFC stack; and the flow and heat transfer conditions are dealt with rationally because of the complex structures of the stack components. The rib channels, cathode support layer, and cathode reaction layer make up the cathode side flow fields of the PCFC stacks. Only the cathode reaction layer contains the heat source in the calculation. The entire stack flow field is determined by the continuity and momentum equations.

$$\nabla \cdot (\rho u) = 0 \quad (1)$$

$$\nabla \cdot (\rho u \times u) = -\nabla P + \rho f + \mu \left(\frac{1}{3}\nabla(\nabla \cdot u) + \Delta u\right) \quad (2)$$

where P, ρ, $\boldsymbol{u}$, are the fluid static pressure, density, and velocity vector, respectively. The ideal air mixing law can be used to compute the effective dynamic viscosity μ.

$$\mu = \sum_{\alpha=1}^{n} \frac{\chi_\alpha \mu_\alpha}{\sum_{\beta=1}^{n} \chi_\beta \Phi_{\alpha,\beta}} \quad (3)$$

Sutherland law with three coefficients is used to determine μ_α at operation temperature T.

$$\mu_\alpha \approx \mu_0 \left(\frac{T}{T_0}\right)^{\frac{3}{2}} \frac{T_0+S}{T+S} \quad (4)$$

where μ is the viscosity in kg m^{-1}s^{-1}, T is the working temperature, μ_0 is reference value at reference temperature T_0 in K, S is an effective temperature in K (Sutherland constant).

The following equation can be used to calculate the concentrations of oxygen, nitrogen, and vapor created by diffusion in the rib channels, porous cathode current collector layers, and cathodic functional layers.

$$\nabla \cdot (\varepsilon \rho Y_\alpha u) = \nabla \cdot \left(\rho D_{\alpha,eff} \nabla Y_\alpha\right) + S_\alpha \quad (5)$$

where ε is the porosity of the porous medium. Y_α and $D_{\alpha,\text{eff}}$ are the mass fraction and effective diffusion coefficient of species α, S_α is the species source item [30]. For the cathode functional layers of the PCFC stack, it can be represented as,

$$S_{O_2} = -\frac{i_{op} M_{O_2}}{4Fl}, \quad S_{H_2O} = \frac{i_{op} M_{H_2O}}{2Fl}, \quad S_{N_2} = 0, \quad (6)$$

M_α is the molar mass of species α, Faraday constant F, and l represents the thickness of the cathode functional layer.

For boundary conditions in the inlet manifolds, inlet velocity will be evaluated by,

$$u_{\text{air}}^{\text{in}} = \frac{Ni_{\text{op}}AM_{air}}{4F\eta_{O_2}\chi_{O_2}\rho_{air}A_{air}} \quad (7)$$

The oxygen mole fraction χ_{O_2} is made up of 21 % oxygen and 79% nitrogen.

Generally, these performance indexes can be used to assess the performance of the cathode airflow designs in the 15-cells PCFC stack.

a) *The normalized air flow rate:* it is derived as $m_i' = m_i/ave(m_1{:}m_N)$. It is easier to compare the distribution performance among different stack sizes, architectures, and operating conditions when the normalized numbers are adopted. Using the average flow rate of the different layers, the normalized data would be derived.

b) Stack pressure drop: The pressure difference between the stack manifold entrance and exhaust exit is also an important consideration when assessing the stac overall design excellence. A big pressure drop increases energy loss, whereas a slight drop may lead to a decrease in oxygen delivery.

c) Minimum flow rate among the piled cells: The performance index *U* measures the flow distributing uniformity by finding the layer that receives the minimum air flow rate $U = min(m_1'{:}m_N')$. Thus, higher values of U indicate a higher uniformity.

3. RESULT AND DISCUSSION

The simulated distributions of the oxygen within the 15-cells PCFC stacks with U and Z configurations are shown in **Fig. 4a** and **b**, respectively. A higher oxygen concentration in the cell layer close to the U-type configuration entrance decreases as we move away from the input. On the other hand, the Z type shows the opposite, as the higher concentration is in the layer farthest from the input. The vapor mole fraction distribution is further analyzed in **Figs. 4c** and **d.** The high flow rates contribute to the water removal; and most of the vapors are found around the outlet manifolds of both the U- and Z-types. Thus, the areas with high flow rates have quality water removing capability, especially from cells 1-9. The results are similar to the results reported in Ref. [31].

Fig. 5a shows that the pressure distributions within both the inlet and outlet manifolds exhibit similar trends in moving in the same direction for the U-type configuration. They increase in the flow direction as the cell number increases in both the inlet and outlet pipes. The Z-type configuration in **Fig. 5b**, however, has the pressure decreasing in the inlet pipes and increasing in the outlet pipes. This outcome is in line with the findings in O-SOFC stack too [14]. A high pressure difference from the 9-th to the 15-th layer causes an uneven distribution in the pile PCFC units with the Z configuration.

Generally, the normalized mass flow rate makes comparing the performance among stacks easier. **Fig. 6** shows the normalized mass flow rate distribution for both the 15-cells U- and Z-configuration PCFC stacks. The airflow feeding quality is a more uniform distribution for the U-type than that of the Z-type configuration stack. It implies that the U-type with the inter-parallel flow field will ensure sufficient oxygen supply to each PCFC layer better than that of Z-type configuration. Thus, the inter-parallel flow field favors the U-type more than the Z-type configuration in a typical planar PCFC stack.

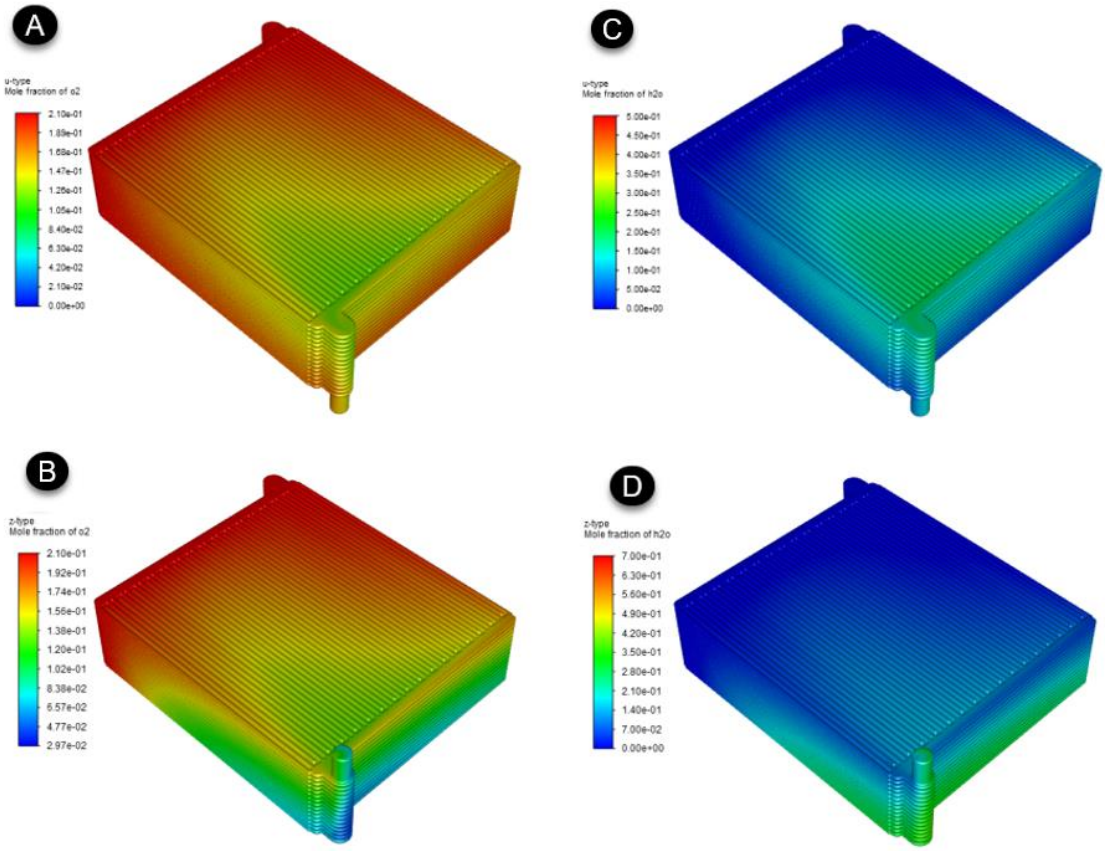

Figure 4. Mole fraction distributions within the 15-cells PCFC stacks, a) Oxygen mole fraction in U-type configuration, b) Oxygen mole fraction in Z-type configuration, c) Water mole fraction in U-type configuration, d) Water mole fraction in U-type configuration.

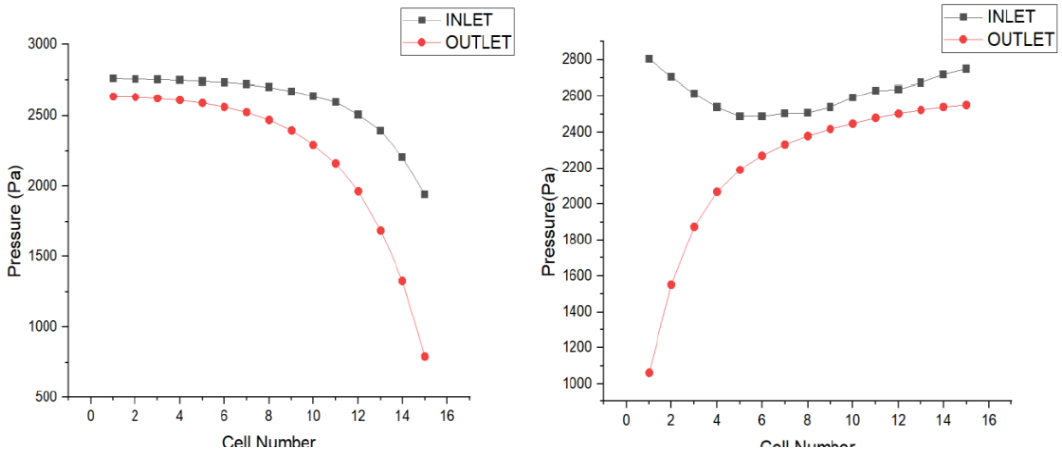

Figure 5. The inlet and outlet pressure distribuitons, a) U-type configuration, b) Z-type configuration.

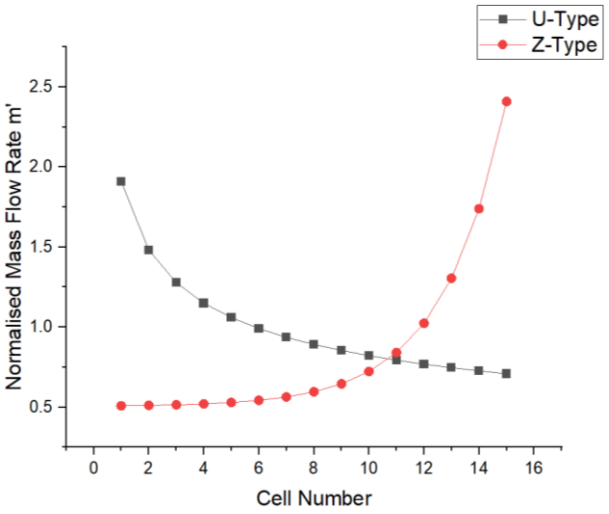

Figure 6. Normalized mass flow rate distributions within the 15-cells PCFC stacks with both the U- and Z-type configuration airflow paths.

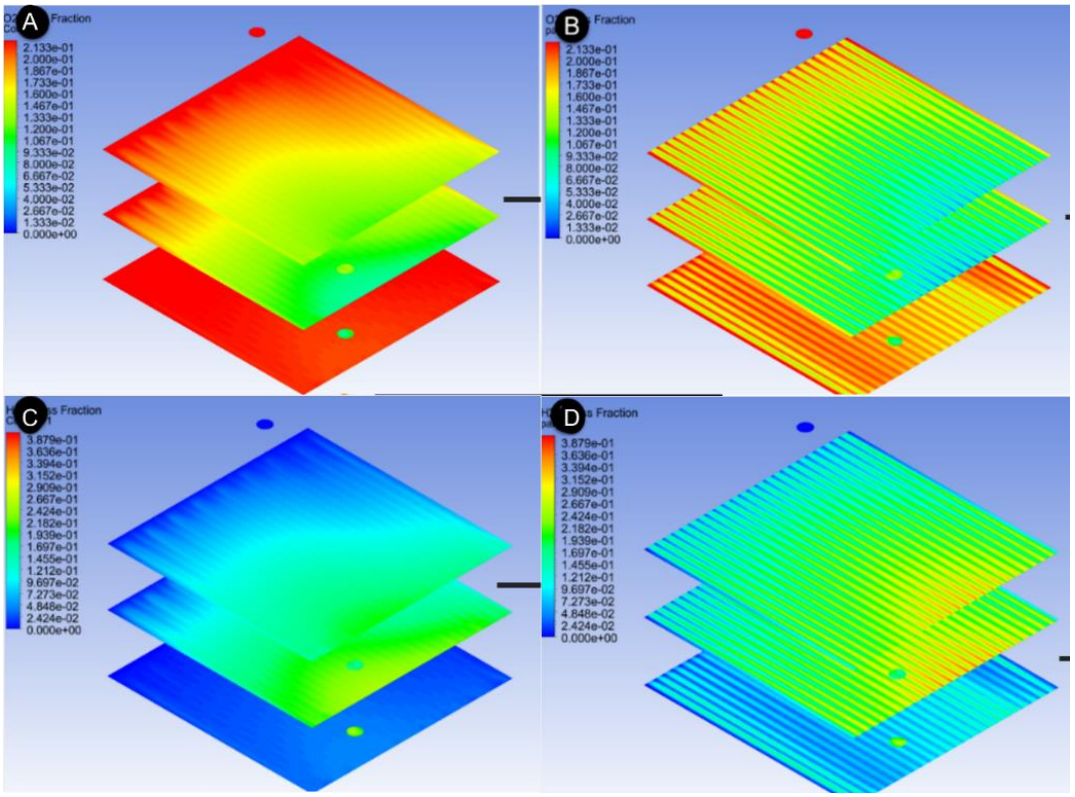

Figure 7. Contours of the mass fraction over the cathode-electrolyte interface, a-b) oxygen mass fraction for the inter-parallel flow field and parallel flow field stacks, respectively, c-d) water mass fraction forinter-parallel flow field and parallel flow field stacks, respectively.

The under rib is one of the most vital parts of our design. It aids especially in water removal and is an advantage over the other flow fields on the stack operating condition. It will be further emphasized by comparing a stack modelled with the inter-parallel flow field and a stack with the parallel flow field.

Since water removal is essential to the high PCFC performane, the mass fraction distribuitons for the stacks with the inter-parallel flow field and the parallel flow fields are compared. **Fig. 7** presents the corresponding first, middle, and last support layers. The PCFC stack using inter-parallel flow field clearly shows the relevance of the under ribs, as more waters are eliminated in these layers than that in the PCFC stack withi parallel flow field. The inter-parallel flow field also has a higher average oxygen concentration over the cathode/dense electrolyte interface than that in the parallel flow field.

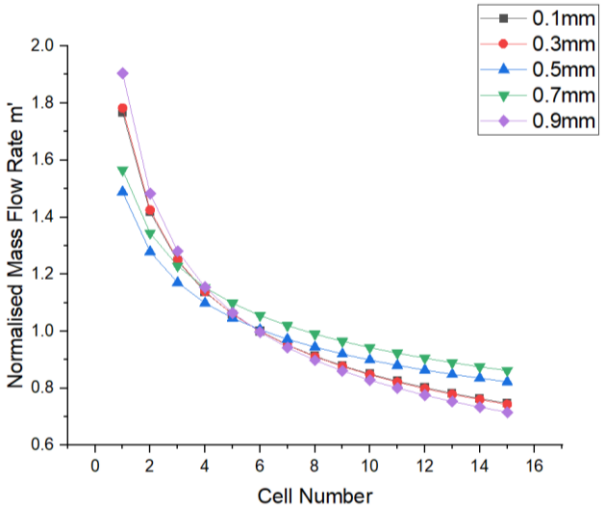

Figure 8. Normalized mass flow rate distributions within the 15-cells PCFC stacks with different geometric parameters.

As previously described, the 15-cells PCFC stack with the under-rib convection may aid in the consistency of airflow distribution among the piled cell units. The 3D CFD models will be used to explore the sensitivities of the PCFC stack flow and species distributions on the geometric characteristics. The effects of the depth of the under-rib channel (shown in **Fig. 1c**) on the flow distribution of the 15-cells PCFC stack will be elucidated to obtain an optimal value. This analysis use the depths of 0.1,0.3, 0.5, 0.7, and 0.9 mm. From **Fig. 8**, the depth of 0.7 mm has the highest index of 0.86, followed by 0.5 mm (*U*= 0.82), 0.3 mm (U = 0.74), and 0.1 mm (0.74). 0.9 mm has the lowest U = 0.71. The results suggest that despite deeper depth will result in a high uniformity, too deep a channel close to the support layer will yield poorer outcomes. The results are validated because it is easier for more reactant and products to reach the reaction areas faster in deeper than in shallow depths.

4. CONCLUSION

In this paper a 3D CFD model for a planar 15-cells planar PCFC stack with the new inter-parallel flow field channel has been well established. Then the dependence of the flow and species distribuitons on the geometric parameters have been investigated; and the following conclusions are obtained.

i) A PCFC stack modeled with the inter-parallel flow field will perform better with the U-type airflow path than the Z-type.

ii) The under-rib convection is critical in our design in ensuring proper flow and reactant transporting and water removing capacities at a low-pressure drop.

iii) The rib channel depth of the current inter-parallel flow field should neither be too deep nor too shallow. A depth of 0.7 mm would be a proper size for the current PCFC stack with inter-parallel flow field.

The results obtained in this research serve as a benchmark for experimental and design work on PCFC stacks with inter-parallel channels.

ACKNOWLEDGEMENTS
We gladly acknowledge the support of the National Natural Science Foundation of China (51776092), the Ministry of Science and Technology of China (CU03-10), and the Jiangsu Province Department of Education.

References

1. J.H. Shim, *Nat. Energy*, 3 (2018) 168-169.
2. M. Zhu, Z. Yang, Z. Han, A. Ishutkin, A. Raza, Z. Yu, D. Chen, *Int. J. Electrochem. Sci*., (2022), 220667.
3. J. Kim, S. Sengodan, S. Kim, O. Kwon, Y. Bu, G. Kim, *Renewable Sustainable Energy Rev*., 109 (2019) 606-618.
4. H. Zhang, Y. Zhu, Z. Chen, L. Lu, A. Levtsev, D. Chen, *Int. J. Hydrogen Energy*, (2022) https://doi.org/10.1016/j.ijhydene.2022.1002.1238.
5. H. Chen, F. Wang, W. Wang, D. Chen, S.-D. Li, Z. Shao, *Appl. Energy*, 179 (2016) 765-777.
6. C. Duan, R.J. Kee, H. Zhu, C. Karakaya, Y. Chen, S. Ricote, A. Jarry, E.J. Crumlin, D. Hook, R. Braun, N.P. Sullivan, R. O'Hayre, *Nature*, 557 (2018) 217-222.
7. K.J. Albrecht, A. Dubois, K. Ferguson, C. Duan, R.P. O'Hayre, R.J. Braun, *J. Electrochem. Soc*., 166 (2019) F687-F700.
8. E.-K. Shin, E. Anggia, A.S. Parveen, J.-S. Park, *Int. J. Hydrogen Energy*, 44 (2019) 31323-31332.
9. L. Blum, L.G.J. de Haart, J. Malzbender, N.H. Menzler, J. Remmel, R. Steinberger-Wilckens, *J. Power Sources*, 241 (2013) 477-485.
10. A.K. Galwey, *React. Kinet. Mech. Catal*., 114 (2015) 1-29.
11. A.J. Samson, P. Hjalmarsson, M. Søgaard, J. Hjelm, N. Bonanos, *J. Power Sources*, 216 (2012) 124-130.
12. H. Zheng, Y. Tian, L. Zhang, B. Chi, J. Pu, L. Jian, *J. Power Sources*, 383 (2018) 93-101.
13. M.A.R.S. Al-Baghdadi, H.A.K.S. Al-Janabi, *Int. J. Hydrogen Energy*, 32 (2007) 4510-4522.
14. D. Chen, Y. Xu, M.O. Tade, Z. Shao, *ACS Energy Lett*., 2 (2017) 319-326.
15. D. Chen, K. Ding, Z. Chen, T. Wei, K. Liu, *Energy Convers. Manage*., 178 (2018) 190-199.
16. R. Boddu, U.K. Marupakula, B. Summers, P. Majumdar, *J. Power Sources*, 189 (2009) 1083-1092.
17. J.P. Owejan, J.J. Gagliardo, J.M. Sergi, S.G. Kandlikar, T.A. Trabold, *Int. J. Hydrogen Energy*, 34 (2009) 3436-3444.
18. R.S. Gemmen, C.D. Johnson, *J. Power Sources*, 159 (2006) 646-655.
19. D. Chen, Y. Zou, W. Shi, S. Serbin, H. You, *Int. J. Energy Res*., 45 (2021) 9948-9960.
20. Y. Xu, A. Kukolin, D. Chen, W. Yang, *Appl. Sci.-Basel*, 9 (2019) 1190.
21. Y. Yang, Y.C. Liang, *J. Power Sources*, 194 (2009) 712-729.

22. Y. Zhang, P. Zhang, Z. Yuan, H. He, Y. Zhao, X. Liu, *J. Power Sources*, 196 (2011) 3255-3259.
23. C. Xu, T.S. Zhao, *Electrochem. Commun*., 9 (2007) 497-503.
24. K. Park, H.M. Kim, K.S. Choi, *Fuel Cells*, 13 (2013) 927-934.
25. J.H. Nam, K.-J. Lee, S. Sohn, C.-J. Kim, *J. Power Sources*, 188 (2009) 14-23.
26. K.S. Choi, B.G. Kim, K. Park, H.M. Kim, *Fuel Cells*, 12 (2012) 908-938.
27. D. Tehlar, R. Flückiger, A. Wokaun, F.N. Büchi, *Fuel Cells*, 10 (2010) 1040-1049.
28. Y.-G. Yoon, W.-Y. Lee, G.-G. Park, T.-H. Yang, C.-S. Kim, *Int. J. Hydrogen Energy*, 30 (2005) 1363-1366.
29. Y.D. Akenteng, X. Yang, Y. Zhao, A. Lysyakov, A. Matveev, D. Chen, *Ionics*, 28 (2022) 3367-3378.
30. K. Ding, M. Zhu, Z. Han, V. Kochetov, L. Lu, D. Chen, *Ionics*, 26 (2020) 4567-4578.
31. J.Q. Dai, Z.M. Yang, W.S. Wang, J.P. Liu, Y.D. Akenteng, D.F. Chen, *Ionics*, 28 (2022) 1863-1872